



ELSEVIER

Spectrochimica Acta Part B 57 (2002) 137–146

SPECTROCHIMICA  
ACTA  
PART B

www.elsevier.com/locate/sab

# Diode laser-aided diagnostics of a low-pressure dielectric barrier discharge applied in element-selective detection of molecular species

K. Kunze<sup>a</sup>, M. Miclea<sup>a</sup>, G. Musa<sup>b</sup>, J. Franzke<sup>a</sup>, C. Vadla<sup>c</sup>, K. Niemax<sup>a,\*</sup>

<sup>a</sup>*Institute of Spectrochemistry and Applied Spectroscopy (ISAS), Bunsen-Kirchoff-Strasse 11, 44139 Dortmund, Germany*

<sup>b</sup>*National Institute for Laser, Plasma and Radiation Physics, 76900 Bucharest-Marguele, Romania*

<sup>c</sup>*Institute of Physics, Bijenicka 46, HR-10000, Zagreb, Croatia*

Received 16 July 2001; accepted 18 September 2001

## Abstract

A small, low-pressure dielectric barrier discharge used as a detector for the analysis of halogenated hydrocarbons was studied by diode laser absorption spectroscopy of excited plasma atoms. The distribution, as well as diffusion of the excited atoms, was measured with high spatial and temporal resolution. The major part of the excited atoms was found in a very narrow discharge volume, where the maximum gas temperature and electron density, determined from broadening of the absorption line profiles, were approximately 1000 K and greater than  $10^{15} \text{ cm}^{-3}$ , respectively. © 2002 Elsevier Science B.V. All rights reserved.

**Keywords:** Dielectric barrier discharge; Diode laser absorption spectrometry; Plasma diagnostics; Halogenated hydrocarbons

## 1. Introduction

We recently reported on the application of a small, low-pressure dielectric barrier discharge (DBD) for the analysis of  $\text{CCl}_2\text{F}_2$ ,  $\text{CClF}_3$  and  $\text{CHClF}_2$  by diode-laser atomic absorption spectrometry (DLAAS) of chlorine and fluorine [1]. It was demonstrated that the analytical figures of merit of DLAAS in a DBD are comparable with data obtained using microwave-induced plasmas (MIP), although the DBD was operated at much lower power ( $<1 \text{ W}$ ) than for MIPs. It was particularly surprising that the DBD was found to

be very efficient for dissociation of the halogenated hydrocarbons.

The present paper is devoted to plasma diagnostics of the low-pressure DBD. This is a challenging task, since the electrode distance of the discharge is very small (1 mm) and the processes in the AC plasma are highly transient. Although DBDs close to atmospheric pressure are widely used, for example, in flat-panel plasma displays for color TV screens [2] or for industrial production of ozone [3], the plasma processes are yet not fully understood. There are only a few papers on the plasma diagnostics of atmospheric DBDs, but to the best of our knowledge, there are no detailed investigations on low-pressure DBDs, such as those used for the analysis of halogenated hydrocarbons.

\* Corresponding author. Fax: +49-231-1392-310.

E-mail address: niemax@isas-dortmund.de (K. Niemax).

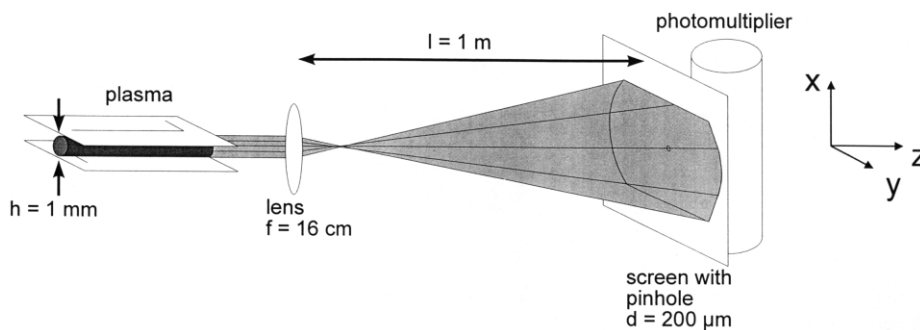


Fig. 1. Experimental arrangement for diode laser absorption measurements of high spatial resolution.

Diode-laser absorption spectroscopy was used for plasma diagnostics of an argon DBD. The measurements were performed with high spatial and temporal resolution (40  $\mu\text{m}$  and 10 ns, respectively). They provided not only the excited-state distribution of short- and long-lived Ar atoms and the diffusion of the metastable atoms, but also the gas temperature and electron density from the analysis of Doppler and Lorentzian line broadening.

## 2. Experimental

The DBD is the same as was used in our experiment on the analysis of  $\text{CCl}_2\text{F}_2$ ,  $\text{CClF}_3$  and  $\text{CHClF}_2$  by DLAAS [1]. The DBD was generated between two glass plates, each with 50 mm long and 0.8 mm wide aluminum electrodes covered by a 20  $\mu\text{m}$  thick glass layer. The distance between the electrodes, including the dielectric layers, was 1 mm (Fig. 1). The DBD device was operated in an argon atmosphere at pressures between 10 and 50 mbar with gas flow-rates between 50 and 500 ml/min. The discharge was sustained by rectangular AC-voltage of 750 V<sub>pp</sub> with a frequency of 5 kHz and rise times of approximately 2  $\mu\text{s}$ . The half-widths of the current pulses were approximately 10  $\mu\text{s}$ . During the pulses, the plasma filled the whole volume between the electrodes. A more detailed description of the experimental arrangement can be found in [1].

Absorption measurements were performed with a single-mode laser diode (Sharp LTO16MDO; line width, approx. 45 fm) tuned to either the

800.836 or the 801.699 nm argon line belonging to the  $1s_4 \rightarrow 2p_6$  and  $1s_5 \rightarrow 2p_8$  transitions, respectively, providing the time-dependent optical depths  $K(t) = \ln[I_0/I(t)]$ , where  $I_0$  is the incident and  $I(t)$  the transmitted laser intensity. Typical transient signals  $I(t)$ , together with the current pulse of the discharge, are shown in Fig. 2. The optical depths are proportional to the concentrations of the argon atoms, either in the resonant  $1s_4$  or the metastable  $1s_5$  state. Investigations of the spatial atomic distribution in the small plasma layer between the electrodes require a spatial resolution of better than 100  $\mu\text{m}$ . For this purpose, we used an optical arrangement that is shown in Fig. 1. The widened beam of the laser diode, directed through the discharge zone parallel to the DBD glass plates and expanded by a lens ( $f = 16$  cm), fell on a screen with a pinhole (diameter 0.2 mm). The intensity of the laser light passing through the pinhole was detected by a photo-multiplier (Hamamatsu). The distance between the lens and screen was 1 m. With this arrangement, it was possible to measure the absorption of a plasma volume with a diameter of approximately 40  $\mu\text{m}$  parallel to the DBD glass plates. A similar optical arrangement, using a hollow cathode as a light source, was already presented in [4].

The absorption signals were measured stepwise by moving the screen with the pinhole in the direction perpendicular ( $x$  direction) and parallel ( $y$  direction) to the DBD glass plates. In this way, the time-dependent spatial absorption distributions  $K(x, y, t)$  with a spatial resolution of  $40 \times 40$   $\mu\text{m}$  in the  $x$ - $y$  plane were obtained. The measurements

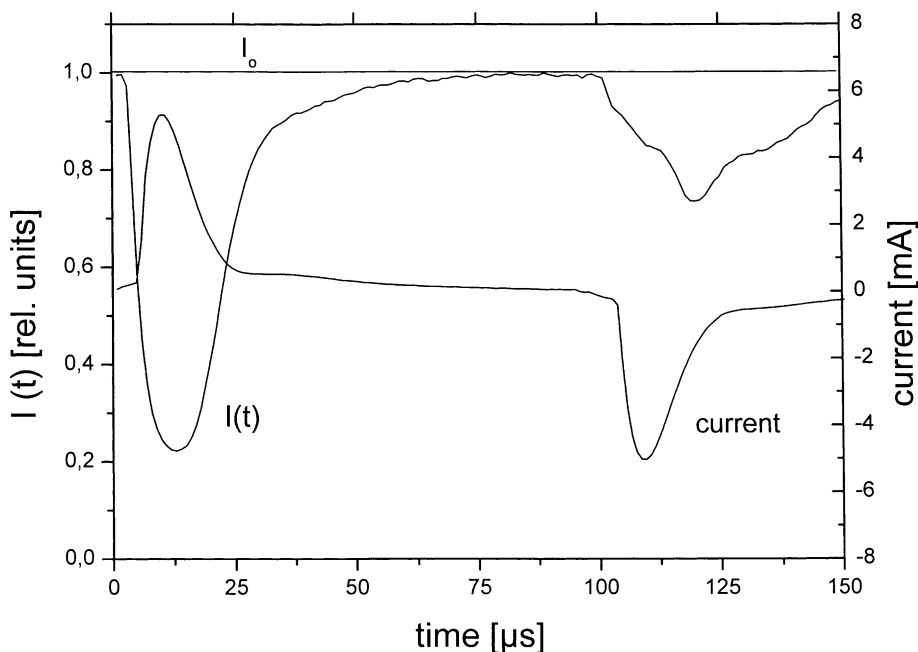


Fig. 2. Discharge current and absorption signals obtained for Ar atoms in the resonance state near to one electrode.

were performed for two orientations of the DBD with respect to the observation axis ( $z$ -axis). In the first case, the plasma column was orientated perpendicular to the observation axis (side-on measurements), whereas in the second case, the plasma column was orientated parallel to the observation axis (end-on measurements).

### 3. Time-dependent and spatial distributions of excited plasma atoms

In the case of side-on measurements, the length of the absorbing layer was approximately 1 mm long and the absorption lines were optically thin, with maximum optical depths of approximately 0.06 and 0.28 for the 800.836 and 801.699 nm lines, respectively. The optical depths  $K_r$  and  $K_m$ , related to the argon atoms excited to the resonance and metastable state, respectively, were strongly dependent on the position  $x$  between the electrodes, while they were constant along the plasma column.

The optical depths  $K_r(x, y=0, t)$  and  $K_m(x, y=0, t)$  measured for one full discharge cycle at an argon pressure of 20 mbar are shown in Fig. 3. In

each half-period, the absorption shows a maximum located at approximately 300  $\mu\text{m}$  from one of the electrodes, which is identified as the temporary cathode. At this position, the highest concentrations of Ar atoms in their resonance and metastable state appear at approximately 12 and 17  $\mu\text{s}$ , respectively, after the polarity changes. The different delays are obviously due to different excitation mechanisms for the  $1s_4$  and  $1s_5$  states. The resonance state is populated by electron impact and recombination and relaxation processes, while only recombination and relaxation are important for the metastable state. Furthermore, it is evident in Fig. 3 that the concentration of metastable atoms decreases much more slowly than the concentration of atoms in the resonance state. This is a consequence of the different lifetimes. The natural lifetime of the Ar  $1s_4$  resonance state is 7.9 ns [5], while it is 55.9 ns for the metastable  $1s_5$  state [6]. However, the actual lifetimes greatly vary from the natural lifetimes under the experimental conditions chosen. Radiation trapping of the argon resonance line increases the actual lifetime of the resonance state, while the lifetime of the metasta-

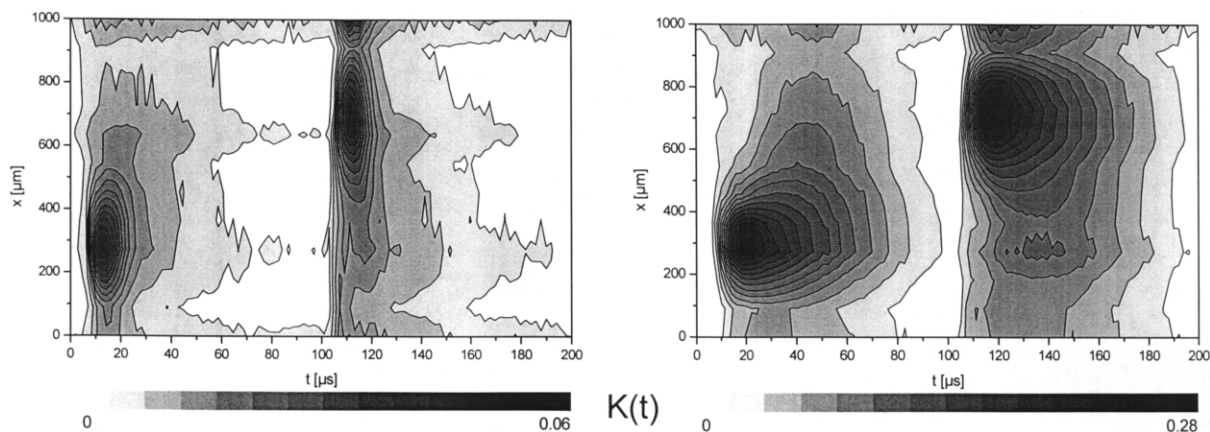


Fig. 3. Time dependence of the peak absorption of Ar measured side-on at different positions between the electrodes (pressure 20 mbar, gas flow 200 ml/min,  $K = \ln[I_0/I(t)]$ ); left, Ar in the resonance state; right, Ar in the metastable state).

ble state is mainly reduced by quenching processes on the near walls of the discharge. The lifetime  $\tau$  of the resonance state can be estimated using the Holstein formula [7]  $\tau_0/\tau = 1.15 \times (\lambda_r/3\pi^2d)^{1/2}$ , where  $\lambda_r$  is the wavelength of the argon resonance line (106.666 nm),  $d$  represents the size of the optically active volume in the form of a thin slab (in our case,  $d \approx 1$  mm), and  $\tau_0$  is the natural lifetime. The value calculated of  $\tau \approx 4$   $\mu\text{s}$  is in agreement with the experimental data obtained by fitting the transient signals to an exponential decay. The actual lifetime of the metastable atoms (approx. 0.1 ms) is still significantly larger than that of the resonance state.

The end-on measurements of  $K_r(t)$  were performed at various argon pressures and in both vertical ( $x$ ) and horizontal ( $y$ ) directions. Fig. 4 shows  $K_r(x, y=0, t)$  measured at two argon pressures (10 and 50 mbar) between the electrodes. The distance between the temporary cathode and the absorption maximum is pressure-dependent. It is approximately 400 and 200  $\mu\text{m}$  for 10 and 50 mbar, respectively. This behavior is similar to the situation in a glow discharge, where the negative glow is shifted towards the cathode if the pressure increases. Furthermore, Fig. 4 shows that the absorption maximum is shifted towards the temporary anode after the discharge current has peaked. This effect should be due to excitation processes caused by a much weaker second dis-

charge maximum at 37  $\mu\text{s}$ , which is barely evident in Fig. 2.

In order to determine the plasma distribution outside the region between the electrodes,  $K_r(x_{\text{max}}, y, t)$  was measured. As indicated, the data were taken at the  $x$ -position where the highest concentrations were detected at 10 and 50 mbar. The results are displayed in Fig. 5. As already observed in Fig. 4, the concentration of excited atoms depends on the pressure, and at lower pressure, the distributions are broader. However, the excited atoms are mostly confined to the region between the electrodes. Therefore, the shift of the absorption maximum in the  $x$ -direction cannot be caused by the diffusion of atoms. On the other hand, the excited atoms outside the electrode region indicate the extension of the plasma at lower pressures, i.e. the diffusion of free electrons in the  $y$ -direction.

#### 4. Plasma diagnostics

The results presented in the previous section show that excited atoms are mainly generated in a very thin layer near the temporary cathode. Therefore, the time-dependent and spatially non-homogeneous discharge is a rather challenging system for plasma diagnostics of the gas temperature and the electron density. These data were obtained by analysis of the absorption profile of the Ar 800.836

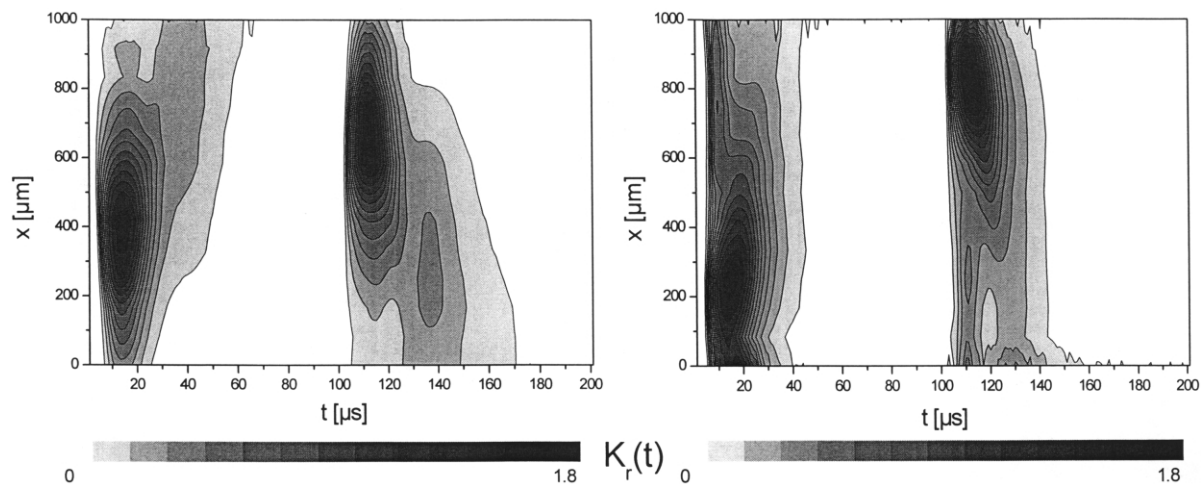


Fig. 4. Time dependence of the optical depth  $K_r$  of the 800.836 nm Ar line measured end-on at different positions between the electrodes at 10 (left) and 50 mbar (right).

nm line measured end-on at the position of highest concentration ( $x_{\max}$ ). The optical depth  $K_r(x_{\max}, y=0, t)$  was measured by tuning the laser stepwise in the wavelength region between  $-15$  and  $+15$  pm around the line center at  $\lambda_0$ . In this way a set of data for  $K_r(t)$  with the laser detuning parameter,  $\Delta\lambda = \lambda_0 - \lambda$ , was measured. Typical results obtained for three different laser detunings are shown in Fig. 6. Taking into account the complete data set, the absorption profile  $K_r(\Delta\lambda)$  at particular

times can be constructed, as shown in the inset of Fig. 6.

At this point, it should be noted that the line profiles may be affected by interference effects in the observation plane if the laser beam is not sufficiently spatially filtered. In this case, the variation of the refractive index within the line profile may cause asymmetries in the absorption line measured. Blue, as well as red, asymmetries may be observed. This effect can be very pro-

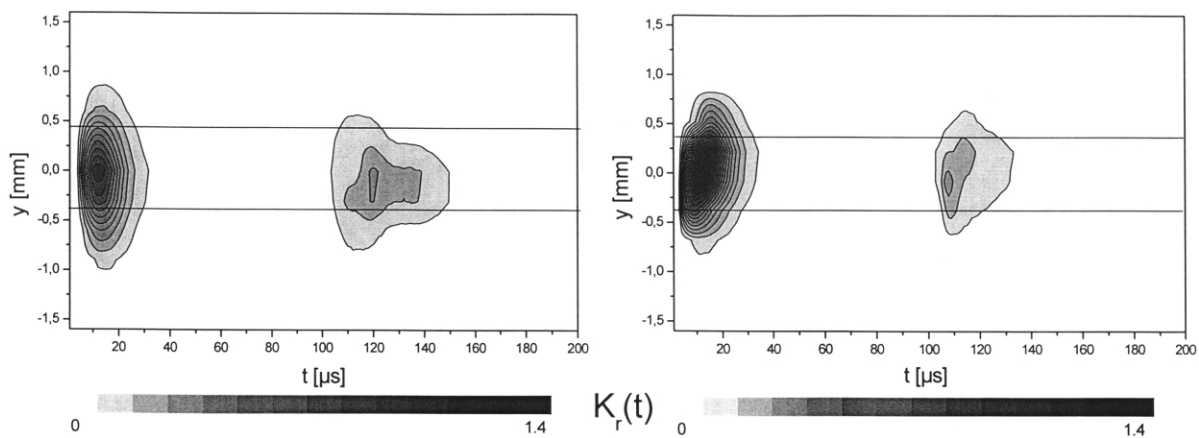


Fig. 5. Time dependence of the optical depth  $K_r$  of the 800.836 nm Ar line measured end-on at the positions of the highest population density at 10 (left) and 50 mbar (right).

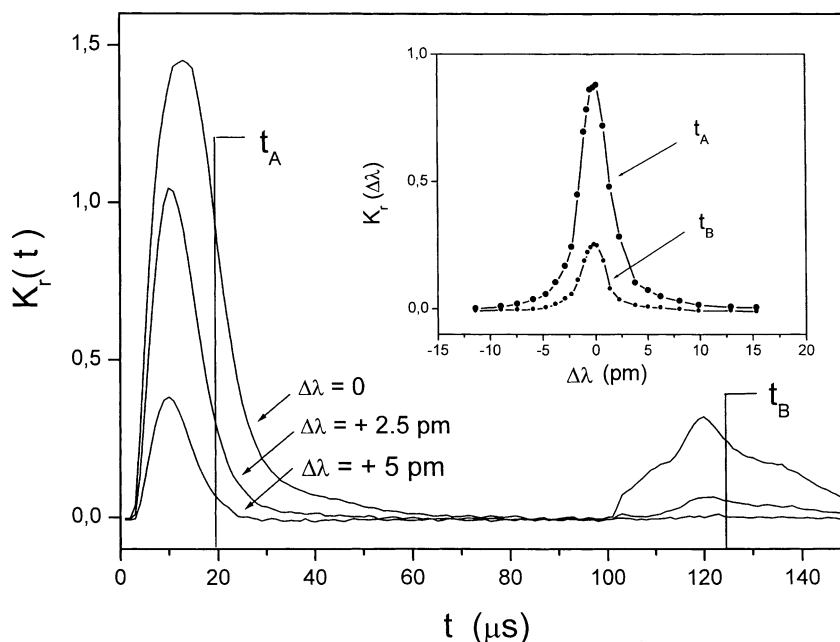


Fig. 6. Procedure for the construction of the 800.836 nm Ar line profiles at different times (for details see text).

nounced if the optical depths in the line centers are greater than 2.

The measurements were performed in the line kernel, where the line profile is generally determined by Doppler and impact broadening and can be analytically described by Gaussian and Lorentzian functions, respectively [8]. The profiles measured for  $K_r(\Delta\lambda)$  are of the Voigt type, i.e. the convolutions of Gaussian and Lorentzian profiles. The shape of the Voigt profile depends on the parameters  $w_G$  and  $w_L$ , which represent the full widths at half-maximum (half-widths) of the Gaussian and Lorentzian contributions, respectively. The half-width  $w_V$  of the Voigt profile is related to  $w_G$  and  $w_L$  according to [9]:

$$w_V = [(w_G)^2 + (w_L/2)^2]^{1/2} + w_L/2 \quad (1)$$

The half-width  $w_G$  of a Gaussian profile gives information on the gas temperature  $T_a$ :

$$w_G = (2\lambda_0/c)(2RT_a \ln 2/M_a)^{1/2} \quad (2)$$

where  $R$  is the universal gas constant and  $M_a$  the mass of the absorbing atoms. On the other hand, the half-width  $w_L$  of the Lorentzian profile is given

by the sum of particular broadening contributions. In DBD, the main contributions are due to interactions between the optically active atoms and the ground-state argon atoms (pressure broadening) and electrons (Stark broadening). Therefore, the actual Lorentzian half-width is of the form  $w_L = w_L^{\text{press}} + w_L^{\text{Stark}}$ .  $w_L^{\text{press}} = \gamma_a N_a$ , where  $\gamma_a$  is the gas temperature-dependent broadening parameter and  $N_a$  the argon density. The Stark-width  $w_L^{\text{Stark}}$  is a complex function of the electron temperature  $T_e$  and the electron density  $N_e$ . The data for  $\gamma_a$  and  $w_L^{\text{Stark}}$  can be found in [10] and [11], respectively.

In order to extract  $w_G$  and  $w_L$  from the absorption coefficients measured, we used a standard method which is based on the fact that the normalized Voigt profiles  $P_V(\Delta\lambda)$  have Lorentzian wings:

$$P_V(\Delta\lambda) \sim (1/2\pi)w_L/(\Delta\lambda)^2 \quad (3)$$

if  $|(\Delta\lambda)| \gg (w_V/2)$ . Then,  $w_L$  can be derived from the profile measured for  $K_r(\Delta\lambda)$  applying:

$$w_L = 2\pi(\Delta\lambda)^2 K_r(\Delta\lambda) / \int K_r(\Delta\lambda) d\lambda \quad (4)$$

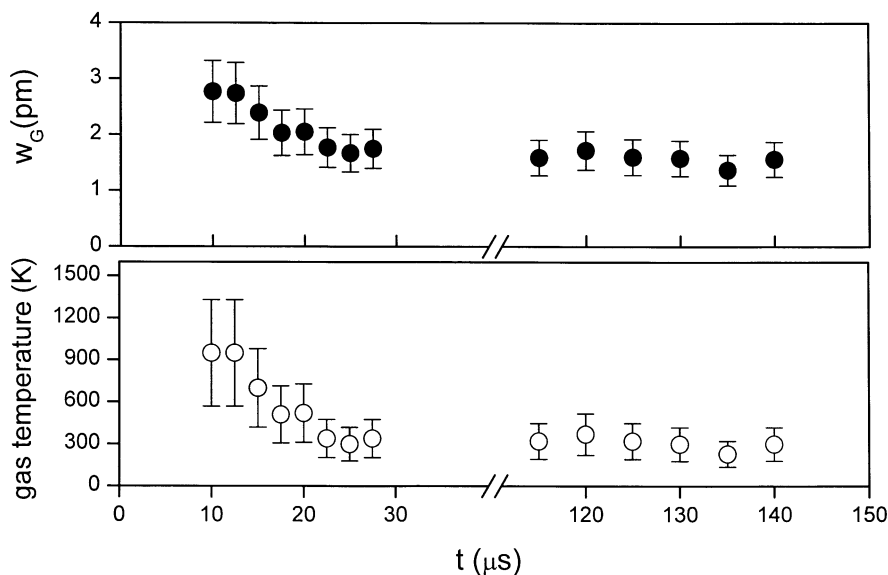


Fig. 7. Time dependence of the Gaussian half-widths  $w_G$  obtained by analysis of the line profiles measured (upper graph). The corresponding gas temperature dependence on time (lower part). The measurements were performed at the position of highest concentration of Ar atoms in the resonance state (near the temporary cathode).

Taking into account the experimental  $w_L$  and  $w_V$ , the corresponding values for  $w_G$  were calculated via Eq. (1).

The time-dependent Gaussian half-widths are plotted in Fig. 7. The data represent the widths measured in the volume of highest population density (at  $x_{\max}$ ). Furthermore, the values calculated for the gas temperature are also displayed in Fig. 7. At the time of maximum excitation, the gas temperature is approximately 1000 K. The gas then cools down to room temperature within 10  $\mu\text{s}$ . During the remaining time of the discharge cycle, the temperature stays constant within the limits of experimental uncertainty, even during the period when the polarity has changed and the second, weaker excitation maximum can be observed.

The time dependence of the Lorentzian width  $w_L$ , displayed in Fig. 8, qualitatively shows similar behavior to the Gaussian width. With the exception of the time of the first discharge maximum,  $w_L$  is constant during the whole discharge cycle ( $w_L \approx 1.7$  pm). Taking into account the experimental error bars, this room-temperature value of  $w_L$  agrees well with the values for pressure-broadening

$w_L^{\text{press}}$  derived from [10]. The contribution of pressure broadening to  $w_L$  for the ‘hot’ discharge period (see Fig. 8) was calculated taking into account the reduced number density in the discharge volume probed (application of Dalton’s law) and the typical temperature dependence ( $\propto T^{0.3}$ ) of the pressure-broadening parameter. The difference between the values measured for  $w_L$  and the  $w_L^{\text{press}}$  data calculated yields the contribution of Stark broadening ( $w_L^{\text{Stark}}$ ) to the measured half-width  $w_L$ . The Stark widths  $w_L^{\text{Stark}}$  are plotted in Fig. 9. Outside the ‘hot’ discharge period, the  $w_L^{\text{Stark}}$  data cannot be evaluated, since the experimental error bars are too large.

The calculation of the electron density from  $w_L^{\text{Stark}}$  requires the electron temperature. Unfortunately, the electron temperatures could not be determined within the scope of the present work. However, taking into account the experimental conditions, the electron temperature should be in the range 10 000–300 000 K. The lower limit of 10 000 K corresponds to the excitation temperature of the resonance and the metastable argon states obtained from the excited to ground-state argon atoms density ratio, while the upper limit is related

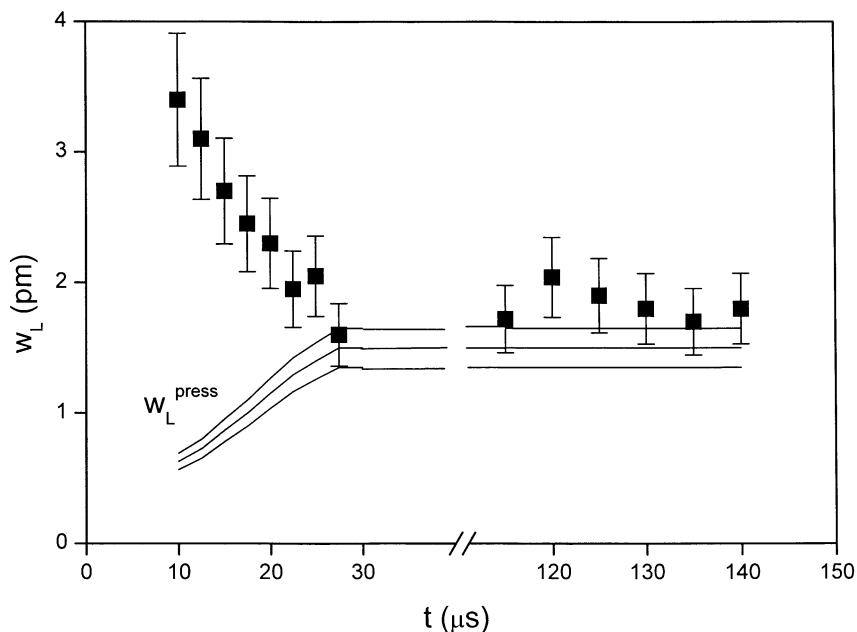


Fig. 8. Time dependence of the Lorentzian half-width of the argon line at 800.836 nm measured at the position of highest concentration of Ar atoms in the resonance state (near the temporary cathode). Furthermore, the contribution from pressure broadening  $w_L^{\text{press}}$  (with upper and lower error bar) is shown. See text for further details.

to the maximum kinetic energy the electrons can accumulate on the average free path in the electric field applied. Nevertheless, this large uncertainty in the experimental electron temperature does not affect the uncertainty of the electron density to the same extent.

The inset in Fig. 9 shows  $w_L^{\text{Stark}}$  in relation to  $N_e$  and  $T_e$  obtained by use of theoretical results published in [11]. The Stark broadening parameters in [11] were calculated for electron temperatures in the range between 2500 and 80 000 K. The dashed curve ( $T_e = 320\,000$  K) in the inset of Fig. 9 is an extrapolation of the theoretical results. Taking into account the experimental error bars and the uncertainty in  $T_e$ , the data in Fig. 9 show that the largest value of  $w_L^{\text{Stark}}$  corresponds to an electron density in the range  $1\text{--}3 \times 10^{15} \text{ cm}^{-3}$ .

Taking into account the maximum electron density of  $1\text{--}3 \times 10^{15} \text{ cm}^{-3}$  and the Ar number density of about  $1.5 \times 10^{17} \text{ cm}^{-3}$  at 20 mbar and 1000 K derived from the ideal gas equation, approximately 1% of all Ar atoms are ionized. The number density of the Ar atoms  $N_{\text{Ar}^*}$  in the metastable and

resonance states can be calculated from the Ladenburg equation:

$$\int K_\lambda d\lambda = \int \ln(I_0/I_\lambda) d\lambda = \frac{\pi e^2}{mc^2} \lambda_0^2 L f N_{\text{Ar}^*} \quad (5)$$

taking into account the side-on measured optical depths  $K_\lambda$  of the 801.699 and 800.836 nm lines, respectively, at the time and position of maximum absorption (see Fig. 3), the approximate absorption length for side-on measurements ( $L = 1$  mm), and the oscillator strength  $f$  of the transitions [5]. The maximum number density values were found to be  $N_{\text{meta}} \approx 1 \times 10^{13}$  and  $N_{\text{res}} \approx 2 \times 10^{12} \text{ cm}^{-3}$ .

## 5. Conclusion

High spatial-resolution plasma diagnostics of low-pressure DBD diode-laser absorption spectroscopy gave clear evidence for a thin, short-lived plasma layer of approximately 40  $\mu\text{m}$  in thickness and 1 mm in width near the temporary cathode. In this layer, plasma atoms are highly efficiently excited, the gas temperature reaches approximately

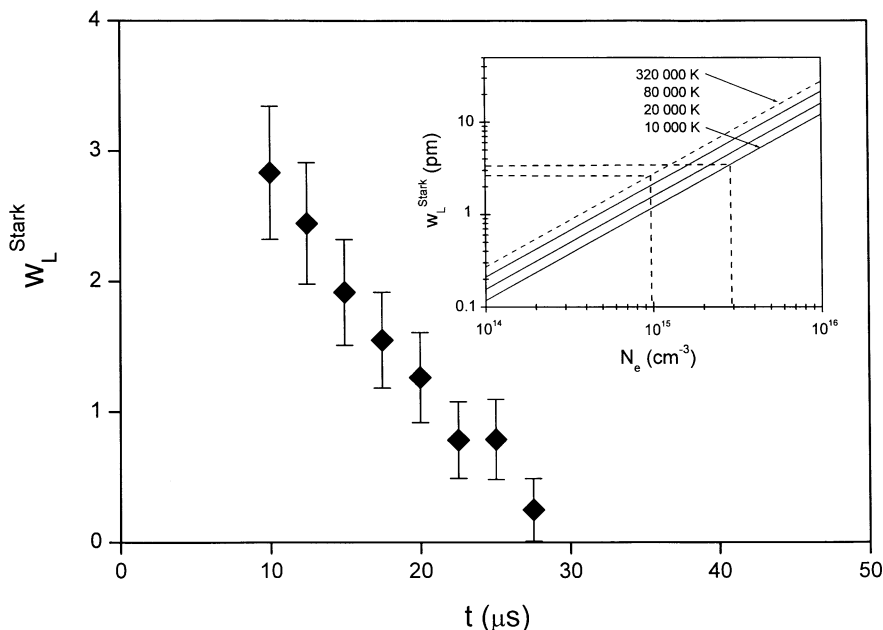


Fig. 9. Time dependence of the Stark width of the 800.836 nm line obtained from the data shown in Fig. 8. Inset shows theoretical values of  $w_L^{\text{Stark}}$  dependent on electron density within the range given by the possible minimum and maximum electron temperatures, 10 000 and 320 000 K, respectively.

1000 K and electron density of greater than  $10^{15}$   $\text{cm}^{-3}$  can be found. In all other areas, the excitation is much less efficient, the gas temperature is near room temperature, and the electron density is below  $10^{14}$   $\text{cm}^{-3}$ . This means that most of the electrical power is used to heat a very small plasma volume. Despite the fact that the average power of the DBD is small ( $\leq 0.1$  W), in this volume the plasma should have an efficient dissociation capability not only for halogenated hydrocarbon, as shown in [1], but also for larger molecules, at least for the main discharge period of approximately 10  $\mu\text{s}$ .

Preliminary diode-laser absorption measurements of excited chlorine in the low-pressure DBD filled with argon and small concentrations of chlorinated hydrocarbons revealed the same spatial distribution as found for excited Ar. As a consequence, the measurements of halogenated hydrocarbons by diode-laser absorption spectroscopy of excited chlorine or fluorine as reported in [1] can be significantly improved. In the former experiment, the diode laser beam filled the whole space

between the electrodes. The main absorption, however, was obviously only due to the small layers near the temporary cathodes. Approximate estimates give an improvement in the detection limit of at least one order of magnitude in comparison to the former experiment if absorption measurements are only restricted to the small area of the plasma layer near the cathodes. Such measurements are now being performed in our laboratory. Furthermore, it is interesting to study the dissociation of molecules in the DBD with high spatial resolution. Such investigation should help to answer the question of whether the DBD is also suitable for dissociation and element-selective detection of larger molecules than halogenated hydrocarbons.

### Acknowledgements

The authors gratefully acknowledge financial support by the Deutsche Forschungsgemeinschaft.

**References**

- [1] M. Miclea, K. Kunze, G. Musa, J. Franzke, K. Niemax, *Spectrochim. Acta Part B* 56 (2001) 37–43.
- [2] T.N. Criscimagna, P. Pleshko, in: J.I. Pankove (Ed.), *Topics in Applied Physics*, 40, Springer Verlag, New York, 1980, pp. 91–150.
- [3] B. Eliasson, U. Kogelschatz, *IEEE. Trans. Plasma. Sci.* 19 (1991) 309–323.
- [4] V. Vadla, M. Movre, R. Beuc, J. Franzke, H.-D. Wize-  
mann, K. Niemax, *Spectrochim. Acta Part B* 55 (2000)  
1759–1769.
- [5] P.L. Smith, C Heise, J.R. Esmond, R.L. Kurucz, Atomic  
spectral line database, in: R.L. Kurucz, CD-Rom 23,  
[http://cfa-www.harvard.edu/amdata/ampdata/  
kurucz23/sekur.html](http://cfa-www.harvard.edu/amdata/ampdata/kurucz23/sekur.html).
- [6] N.E. Small-Waren, C.C. Lue-Yung, *Phys. Rev. A* 11  
(1975) 1777–1783.
- [7] T. Holstein, *Phys. Rev.* 83 (1951) 1159–1168.
- [8] A. Unsöld, *Physik der Sternatmosphären*, Springer Ver-  
lag, Berlin, 1968.
- [9] G.W.F. Drake, *Atomic, Molecular and Optical Physics  
Handbook*, AID Press, Woodbury, NY, 1966, p. 698.
- [10] K. Tachibana, H. Harima, Y. Urano, *J. Phys B: At. Mol.  
Phys* 15 (1982) 3169–3178.
- [11] H.R. Griem, *Plasma Spectroscopy*, McGraw-Hill, New  
York, 1964.